Endothelial cells elicit a pro-inflammatory response to SARS-CoV-2 without productive viral infection

Lilian Schimmel[1*] Keng Yih Chew[2*] Claudia Stocks[3] Teodor Yordanov[1] Tish Essebier[1] Arutha Kulasinghe[4,5] James Monkman [4,5] Anna Flavia Ribeiro dos Santos Miggiolaro[6] Lucia de Noronha[7] Anne K. Lagendijk[1] Kate Schroder[3] Larisa Labzin[3#] Emma J. Gordon[1#] & Kirsty R. Short[2#]

1. Division of Cell and Developmental Biology, Institute for Molecular Bioscience, The University of Queensland, Brisbane, QLD, Australia
2. School of Chemistry and Molecular Biosciences, The University of Queensland, Brisbane, QLD, Australia
3. IMB Centre for Inflammation and Disease Research, Institute for Molecular Bioscience, The University of Queensland, Brisbane, QLD, Australia
4. Queensland University of Technology, School of Biomedical Sciences, Faculty of Health, Brisbane, Queensland, Australia.
5. Translational Research Institute, Brisbane, Queensland, Australia.
6. Postgraduate Program of Health Sciences, School of Medicine, Hospital Marcelino Champagnat - Pontifícia Universidade Católica do Paraná (PUCPR), Brazil
7. School of Medicine & Center of Education, Research and Innovation – Hospital Marcelino Champagnat - Pontifícia Universidade Católica do Paraná (PUCPR). Brazil

*/# authors contributed equally

Correspondence:

k.short@uq.edu.au

e.gordon@imb.uq.edu.au

Running title: SARS-CoV-2 does not productively infect endothelial cells

ABSTRACT

Thrombotic and microvascular complications are frequently seen in deceased COVID-19 patients, suggesting that vascular pathology is a major driver of severe disease. However, whether this is caused by direct viral infection of the endothelium or inflammation-induced endothelial activation remains highly contentious. What role the endothelium plays in viral amplification and inflammation thus remains a key unresolved question in the pathogenesis of SARS-CoV-2.

Here, we use patient autopsy samples, primary human endothelial cells and an *in vitro* model of the pulmonary epithelial-endothelial cell barrier to show that primary human endothelial cells express the SARS-CoV-2 receptor ACE2 and the protease TMPRSS2, albeit at low levels. Accordingly, when present in a sufficiently high concentration, SARS-CoV-2 can enter primary human endothelial cells from either the apical or basolateral surface. Whilst inducing an inflammatory response, this is not a productive infection. We further demonstrate that in a co-culture model of the pulmonary epithelial-endothelial barrier, endothelial cells are not infected with SARS-CoV-2. They do however, sense and respond to an infection in the adjacent epithelial cells, resulting in the induction of a pro-inflammatory response.

Taken together, these data suggest that *in vivo,* endothelial cells are unlikely to be infected with SARS-CoV-2 and that infection is only likely to occur if the adjacent pulmonary epithelium is denuded (basolateral infection) or a high viral load is present in the blood (apical infection). In such a scenario, whilst SARS-CoV-2 infection of the endothelium can occur, it does not contribute to viral amplification. However, endothelial cells are still likely to play a key role in SARS-CoV-2 pathogenesis by sensing and mounting a pro-inflammatory response to SARS-CoV-2.

INTRODUCTION

SARS-CoV-2 causes diverse clinical syndromes, ranging from asymptomatic infection to fatal disease. Of patients hospitalised with COVID-19 (the clinical manifestation of SARS-CoV-2 infection), approximately 30% of individuals go on to develop severe disease associated with progressive lung damage. This is associated with a breakdown of the vascular barrier, oedema, endotheliitis, thrombosis and inflammatory cell infiltration [1, 2]. Many studies have identified thrombotic and microvascular complications in deceased patients, suggesting that vascular pathology is a major driver of severe disease [3, 4]. Other major pathological events include arterial and venous thromboembolism, kidney disease, neurological disorders and diabetes [5, 6], suggesting that SARS-CoV-2 activates the vasculature throughout the body, potentially resulting in multi-organ failure. However, whether this is caused by direct viral infection of the endothelium or inflammation-induced endothelial activation remains highly contentious.

SARS-CoV-2 cellular uptake is mediated by binding of the spike glycoprotein to ACE2 (angiotensin-converting enzyme 2) and NRP1 (Neuropilin-1) at the cell surface [7-10]. Host surface proteases such as TMPRSS2 cleave full-length spike protein (S0) at its S2' site. Cleavage at the S2' site can facilitate the fusion of viral and cellular membranes to deliver the viral RNA into the cytosol [1, 11]. Alternative routes of virus uptake involving the endo-lysosomal pathway and a role for cathepsins in viral-host membrane fusion have also been reported in cells with low expression of TMPRSS2 [12]. Numerous studies suggest that endothelial cells express ACE2 [3, 13-17], Neuropilin receptors [18-22] and TMPRSS2 [23], suggesting that viral infection of endothelial cells is theoretically possible. However, others have suggested that ACE2 is highly expressed in microvascular pericytes of the heart [14, 24] and that pericyte injury in response to viral infection may lead to endothelial dysfunction.

Evidence regarding direct infection of the endothelium with SARS-CoV-2 remains equivocal. Autopsy studies on COVID-19 patients have suggested the presence of viral particles in the vascular beds of different organs [3, 25, 26] and others have shown SARS-CoV-2 infection of cultured endothelial cells [27, 28] and human blood vessel organoids [29]. In contrast, several studies have failed to find evidence

of endothelial infection in deceased COVID-19 patients [30] and called into question the validity of identifying virally-infected cells based on the presence of the SARS-CoV-2 spike protein [31, 32]. Animal models of SARS-CoV-2 infection have also failed to identify any obvious signs of endothelial infection [33, 34], despite clear endothelial dysfunction and thrombosis [35].

When and how endothelial cells may be exposed to SARS-CoV-2 *in vivo* also remains unclear. As a respiratory virus, SARS-CoV-2 encounters pulmonary epithelial cells prior to any interaction with the endothelium. SARS-CoV-2 infects pulmonary epithelial cells apically and new viral particles are also released apically into the lumen of the lung [36]. It is possible that the infected epithelial layer loses barrier function, allowing endothelial infection from the basolateral side of epithelia that is adjacent to alveolar endothelium. Alternatively, SARS-CoV-2 may infect endothelial cells apically via the blood, although viremia appears to be rare in COVID-19 patients [37]. The question therefore remains whether endothelial dysfunction in COVID-19 is the result of direct viral infection of the endothelium.

Here, using patient autopsy samples and *in vitro* models, we show that while endothelial cells can be infected when exposed to high titres of SARS-CoV-2, this infection is not productive. Rather, in response to direct or indirect viral exposure, endothelial cells mount a pro-inflammatory response characterised by increased expression of ICAM-1 and secretion of CXCL-10 and IL-6. Taken together, our results provide clarification on the intensely debated topic of endothelial infection by SARS-CoV-2, to reveal that the endotheliopathy and thrombocytopathy in patients with severe COVID-19 is likely to be due to the inflammatory response mounted by the vasculature, rather than direct viral infection.

MATERIALS AND METHODS

In vivo samples: Lung tissue from 10 SARS-CoV-2 infected patients was sectioned and Hematoxylin and Eosin (H&E) staining performed. RNAscope probes (ACDbio, US) targeting SARS-CoV-2 spike mRNA (#848561-C3), were used as per manufacturer instructions for automation on Leica Bond RX. DNA was visualised with Syto13, and SARS-CoV-2 spike probe with opal 690 (1:1500). Fluorescent images were acquired with Nanostring Mars prototype DSP at 20x. Autopsy and biopsy materials were

obtained from the Pontificia Universidade Catolica do Parana PUCPR the National Commission for Research Ethics (CONEP) under ethics approval numbers 2020001792/30188020.7.1001.0020 and 2020001934/30822820.8.000.0020. The study was also approved under University of Queensland HREC ratification.

Cell culture: Human umbilical vein endothelial cells (HUVECs), and human microvascular endothelial cells from lungs (HMVEC-L) purchased from Lonza (Cat# CC-2935, and CC-2527 respectively) were cultured until passage 8 in EGM-Plus or EGM-2MV medium, supplemented with singlequots (Lonza Cat# CC-5035, CC-3102). Calu-3 cells purchased from ATCC (Cat# HTB-55) were maintained in MEM (Invitrogen), containing 10% (v/v) heat-inactivated foetal bovine serum (Cytiva), 100 U/ml penicillin and streptomycin (Life Technologies Australia), and grown in EGM-2MV for endothelial co-culture experiments.

Monocultures of HUVEC, HMVEC or Calu-3 cells were performed on 24 well cell culture inserts (Corning 6.5 mm Transwell, 0.4 µm polycarbonate membrane Cat#3413) coated with 5 µg/ml FN (Sigma). Approximately 25,000 HUVEC, 25,000 HMVEC and 50,000 Calu-3 cells were seeded per insert on either the apical or basolateral side as indicated and grown in EGM-Plus (Lonza), EGM-2MV (Lonza) or MEM (Invitrogen) respectively. Endothelial cells were treated with 100ng/ml TNFα for 16h as indicated.

Calu-3 and HMVEC were co-cultured on 24 well cell culture inserts (Corning 6.5 mm Transwell, 0.4 µm polycarbonate membrane Cat#3413) coated with 5 µg/ml FN (Sigma) in EGM-2MV (Lonza). Approximately 25,000 HMVECs were seeded on an inverted filter for 1 hr to attach. Filters were turned over to normal position and approximately 50,000 Calu-3 cells were seeded in the top compartment of the filter. Cells were grown for 48 hr prior to infections.

Viral infection: SARS-CoV-2 isolate hCoV-19/Australia/QLD02/2020 was provided by Queensland Health Forensic & Scientific Services, Queensland Department of Health. Virus was grown on Vero cells and titred [38]. Sanger sequencing was used to confirm that no mutations occurred in the spike gene relative to the original clinical isolate. Cells were infected with 6 x 10^4 plaque forming units (PFU)

for 1 hour at 37 degrees 5% Co2. The viral inoculum was then removed, and the medium was replaced with DMEM (Invitrogen) or MEM (Invitrogen) containing 2% FBS. Alternatively, 2 x 10^6 PFUs were added to the cell culture and cells were incubated at 37 degrees 5% CO_2. All studies with SARS-CoV-2 were performed under physical containment 3 (PC3) conditions and were approved by the University of Queensland Biosafety Committee (IBC/374B/SCMB/2020).

Antibodies: The following antibodies were used: mouse anti-ACE2 (Santa Cruz, sc-390851, IF1:200) goat anti-ACE2 (R&D systems, AF933, WB 1:1000), mouse anti-dsRNA (Millipore, MABE1134, IF1:100), rabbit anti-SARS-CoV nucleoprotein/NP (Sino Biological, 40143-R040, WB1:1000 IF1:200), rabbit anti-TMPRSS2 (Abcam, ab92323, WB1:1000), mouse anti-ORF7a (GeneTex, GTX632602, WB1:1000), rabbit anti-GAPDH (Cell Signaling, 2118, WB1:2000), mouse anti-ICAM-1 (R&D systems, BBA3, IF1:200), mouse anti-ICAM-1 (Santa Cruz Biotechnology, sc-8439, WB1:1000), Phalloidin-Alexa555 (Cytoskeleton, PHDH1-A, IF1:500), Phalloidin-Alexa670 (Cytoskeleton, PHDN1-A, IF1:200).

Immunofluorescence Staining: Immunofluorescence staining was in general performed on cells cultured on 12 mm glass coverslips or on 24 well cell culture inserts (Corning 6.5 mm Transwell, 0.4 µm polycarbonate membrane Cat#3413) coated with 5 µg/ml FN (Sigma), washed with $PBS^{+/+}$(PBS supplemented with 1 mM $CaCl_2$ and 0.5 mM $MgCl_2$), fixed for 10 min in 4% PFA (Sigma), blocked and permeabilized for 30 min with 3% BSA, 0.3% Triton X-100 (Sigma). Primary antibodies were incubated in 1.5% BSA for 1 hr at RT, secondary antibodies linked to Alexa fluorophores (all Invitrogen) were incubated in 1.5% BSA for 1 hr at RT and incubated with 4% PFA (Sigma) for another 24 hr in case of SARS-CoV-2 infected cells, after each step samples were washed 3x with $PBS^{+/+}$ and mounted in ProlongGold + DAPI solution (Cell Signaling Technologies, CST 8961S). Z-stack image acquisition was performed on a confocal laser scanning microscope (Zeiss LSM880) using a 40x NA 1.3 or 63x NA 1.4 oil immersion objective.

Western blotting: For total cell lysates, cells were washed once with PBS and lysed with RIPA buffer (50 mM Tris, 150 mM NaCl, 1 mM EDTA, 1% Triton X-100, 0.1% SDS, 1% sodium deoxycholate, protease inhibitor, pH 8.0). Pierce BCA protein assay kit (Thermo Scientific) was used to equalize protein amounts and SDS-sample buffer containing 100 mM DTT (Astral Scientific) was added and samples were boiled at 95°C for 10 minutes to denature proteins. Proteins were separated on 4-15% mini protean TGX precast gels (Biorad) in running buffer (200 mM Glycine, 25 mM Tris, 0.1% SDS (pH8.6)), transferred to nitrocellulose membrane (BioRad Cat#1620112) in blot buffer (48 nM Tris, 39 nM Glycine, 0.04% SDS, 20% MeOH) and subsequently blocked with 5% (w/v) BSA in Tris-buffered saline with Tween 20 (TBST) for 30 minutes. The immunoblots were analysed using primary antibodies incubated overnight at 4°C and secondary antibodies linked to horseradish peroxidase (HRP) (Invitrogen), and after each step immunoblots were washed 4x with TBST. HRP signals were visualized by enhanced chemiluminescence (ECL) (BioRad) and imaged with a Chemidoc (BioRad).

RNA extraction and cDNA synthesis: RNA was extracted using the Qiagen RNeasy Minikit (Qiagen) or NucleoZOL (BIOKÉ, The Netherlands) according to manufacturer's guidelines. cDNA was synthesized using random hexamers and the high-capacity cDNA reverse transcription kit (Life Technologies) according to the manufacturer's guidelines.

Quantitative PCR (qPCR): qPCR was performed using SYBR Green reagent (Applied Biosystems). All primer sequences are listed in Table 1. qPCR conditions were applied according to the manufacturer's instructions using QuantStudio 6 Flex Real- Time PCR System (ThermoFisher Scientific, Waltham, Massachusetts, MA). HPRT or Glyceraldehyde 3-phosphate dehydrogenase (GAPDH) was used as a housekeeping gene and relative gene expression was determined using the comparative cycle threshold (ΔΔCt) method (Livak, 2001).

Table 1: Primers used in the present study

NAME	SEQUENCE (5'- 3')

SARS-COV2 (MPRO) VIRUS FW	GAGACAGGTGGTTTCTCAATCG
SARS-COV2 (MPRO) VIRUS RV	ACGGCAATTCCAGTTTGAGC
GAPDH FW	CGAGATCCCTCCAAAATCAA
GAPDH RV	TTCACACCCATGACGAACAT
HPRT FW	TCAGGCAGTATAATCCAAAGATGGT
HPRT RV	AGTCTGGCTTATATCCAACACTTCG
ACE2 FW	TCACGATTGTTGGGACTCTGC
ACE2 RV	TCGCTTCATCTCCCACCACT
NEUROPILLIN FW	TGGACCGACCACTCCCAACG
NEUROPILLIN RV	AGAGCCCCAGCCAAATTCACAG
TMPRSS2 FW	GGAAGTTCATGGGCAGCAAG
TMPRSS2 RV	AGGCGAACACACCGATTCTC

Viral titres: Viral titres in cell culture supernatant determined by a plaque assay on Vero cells, according to previously described protocols [38].

Cytokine titres: Cytokine titres in were determined using an Alphalisa kit (Perkin Elmer) according to the manufacturer's instructions. The sum of cytokines detected in the upper and lower compartments of the transwell is shown for each of the monocultured samples, while cytokine levels were kept separated for the upper and lower compartment for the co-cultured samples.

Image analysis: Analysis of immunofluorescent images was performed using ImageJ version 2.0.0-rc-69/1.52n. A mask of the total cell area was created using default intensity threshold on Phalloidin staining. Within the mask, Raw Integrated Density of either ACE2, NP, ICAM-1 was measured, and value was corrected for total mask area resulting in RawIntDen/Area. For dsRNA, MaxEntropy threshold was performed on dsRNA staining to remove background speckles before measuring Raw Integrated Density within the mask. Analysis of Western blot images was performed using Gel Analyzer Tool of ImageJ version 2.0.0-rc-69/1.52n. The background signal was subtracted and values were

normalized to corresponding GAPDH loading control. Imaris (Bitplane) version 8 was used to create the XZ projection in Figure 4B''. Extrusion of cells was quantified in Supplemental Figure 1C using orthogonal views in ImageJ version 2.0.0-rc-69/1.52n.

Statistical analysis: All statistical analysis was performed using Graphpad Prism version 9.0. Data are presented as mean±s.e.m. with individual data points indicated and colour coded per independent experimental replicate. Statistical significance was determined using Kruskal Wallis test for multiple comparisons or Mann-Whitney test between mock and SARS-CoV-2 treated conditions. *P<0.05, **P<0.01, ***P<0.001 and ****P<0.0001.

RESULTS

Endothelial cell infection is not readily detected in deceased COVID-19 patients

To determine the prevalence of *in vivo* SARS-CoV-2 endothelial cell infection, autopsy lung sections were obtained from 10 deceased COVID-19 patients and stained for SARS-CoV-2 spike mRNA. In the collected specimens, spike mRNA could not be detected in pulmonary endothelial cells (representative images shown in Figure 1). These data suggest that the endothelium is not generally the primary site of viral replication in COVID-19 patients.

Primary endothelial cells express low levels of ACE2 and TMPRSS2

To further investigate the contribution of endothelial cells to the pathogenesis of SARS-CoV-2, we established *in vitro* cultures of primary human umbilical vein endothelial cells (HUVECs) and human microvascular endothelial cells from the lung (HMVEC-L). Multiple studies have reported that endothelial cells across different vascular beds express ACE2 and TMPRSS2, the host cell receptor and protease that are required for efficient cell infection by SARS-CoV-2 [10, 11]. We found that both HUVECs and HMVEC-Ls expressed comparable ACE2 and TMPRSS-2 mRNA to that observed in immortalised epithelial cells known to be susceptible to SARS-CoV-2 infection (Calu-3) (Figure 2A). Neuropilin-1, which enhances viral entry through its interaction with the spike multibasic cleavage site [7, 8], was readily detected in endothelial cells by qPCR (Figure 2A) in line with established data [19].

We also detected ACE2 (Figure 2B-E) and TMPRSS2 (Figure 2B-C) protein in HUVECs and HMVEC-Ls by western blot, however the expression of ACE2 detected by immunofluorescence (Figure 2D) was significantly reduced compared to epithelial cells [Calu3] (Figure 2E), with a similar trend being observed for both ACE2 and TMPRSS2 by western blot (Figure 2C). These data suggest that while vascular endothelial cells can theoretically be infected by SARS-CoV-2, infection is likely to be inefficient compared to epithelial cells, because of weak receptor and protease expression in endothelial cells.

Endothelial cells are not productively infected by SARS-CoV-2

SARS-CoV-2 may theoretically enter endothelial cells via the apical surface (should the virus enter the blood stream) or the basolateral surface (should the virus be present at the basolateral surface of the adjacent epithelial cells). We therefore assessed whether endothelial cells were susceptible to SARS-CoV-2 infection when exposed either apically (Figure 3A) or basolaterally (Figure 3B) to 6 x 10^4 PFUs. Infectious virus was not detected in the supernatant of either HUVECs or HMVEC-Ls at 24, 48 nor 72 hours post-infection (Figure 3C). In contrast, Calu-3 cells demonstrated robust viral replication and release (Figure 3C; Supplementary Figure 1A). Similarly, no increase in SARS-CoV-2 nuclear protein within infected endothelial cells relative to mock was detected by immunofluorescence (Figure 3D-G) or western blot (Figure 3H-I), and no detectable alterations in endothelial cell morphology were evident after viral exposure, as assessed by phalloidin immunostaining (Figure 3D, F). In contrast, Calu-3 cells displayed a significant increase in nuclear protein expression after viral exposure. Together, these data suggest that endothelial cells *in vitro* are not efficiently infected with SARS-CoV-2.

We next sought to establish if the low levels of ACE2 and TMPRSS2 on endothelial cells could be overcome by a higher viral titre, to mediate infection. Accordingly, endothelial cells were infected either apically or basolaterally with 2 x 10^6 PFUs of SARS-CoV-2 and viral replication was again assessed over time. Viral replication was again undetectable in endothelial cells from 24-72h post-infection, in contrast to Calu-3 cells which displayed robust viral replication (Figure 4A; Supplementary Figure 1B). To determine if endothelial cells were susceptible to viral entry, we assessed viral nuclear protein in

HMVEC-L by immunofluorescence (Figure 4B-C) and western blot (Figure 4D-E). Viral nuclear protein expression was significantly increased after both apical and basolateral SARS-CoV-2 infection compared to mock, revealing that SARS-CoV2 can indeed enter endothelial cells *in vitro*. The majority of infected, nuclear protein-positive endothelial cells appeared to be extruding from the cell monolayer in an apical manner (Figure 4B', B'', Supplemental Figure 1C). These results demonstrate that while endothelial cells can be infected by SARS-CoV-2, in contrast to epithelial cells, infection in endothelial cells is not productive and leads to cell extrusion from the monolayer.

Endothelial cells mount a modest immune response to SARS-CoV-2

As severe COVID-19 disease is associated with an elevated cytokine response [39], we sought to assess whether the abortive SARS-CoV-2 infection observed in endothelial cells induces a pro-inflammatory response. We assessed expression of the leukocyte adhesion molecule, ICAM-1, which is well established to be induced under inflammatory conditions in the endothelium [40]. Immunofluorescence showed that while nuclear protein-positive HMVEC-L did not express elevated ICAM-1 (likely as they are extruding from the monolayer), both basal and apical exposure to SARS-CoV-2 induced a significant increase in ICAM-1 expression in the remaining endothelial cells (Figure 5A-C). However, this response was not as robust as when HMVEC-L were exposed to the established inflammatory cytokine TNFα (Figure 5B-C). Western blot analysis confirmed that HMVEC-L exposed to SARS-CoV-2 displayed a trending increase in ICAM-1 expression (Figure 5D, E). In addition to upregulating inflammatory adhesion molecules, we analysed whether endothelial cells can be source of pro-inflammatory cytokines during SARS-CoV-2 infection. As IL-6 and CXCL10 are elevated in patients with severe COVID-19 [41], we analysed whether endothelial cells released these pro-inflammatory cytokines upon SARS-CoV-2 infection. While endothelial cells released modest levels of CXCL10 72h after apical SARS-CoV-2 infection (Figure 5F), IL-6 secretion was markedly induced in HMVEC-Ls infected either apically or basolaterally (Figure 5G). Taken together, these results show that endothelial cells do not support a productive SARS-CoV-2 infection but still mount a modest pro-inflammatory response to the virus.

Infection of epithelial-endothelial co-cultures elicits an immune response in endothelial cells

To create a more physiologically relevant *in vitro* model of the pulmonary endothelium, we adapted our previously described co-culture model of the lung epithelial-endothelial barrier [42], where epithelial (Calu-3) cells are seeded on top of a transwell membrane while endothelial cells (HMVEC-L) are seeded on the basolateral side. To mirror a respiratory infection, SARS-CoV-2 was added to the upper compartment and both epithelial and endothelial cells were analysed at 72h post-infection. In contrast to our observations in endothelial cell monocultures, no viral nuclear protein or viral dsRNA was detected in HMVEC-L, whereas SARS-CoV-2 protein and RNA was clearly detected in infected Calu-3 cells (Figure 6A-G). These results were confirmed by the presence of infectious virions in the upper, but not the lower, compartment of the transwell (Figure 6H). Despite lack of endothelial infection, ICAM-1 expression was induced in HMVEC-L in response to virus (Figure 6A, D). HMVEC-L responded to the adjacent infected epithelia by producing CXCL10 (detected in lower compartment of the co-culture) (Figure 6I). However, unlike results from HMVEC-L monocultures, IL-6 secretion was only significantly elevated in the upper compartment of infected co-cultures, with only a trend towards increased IL-6 secretion from the lower compartment of the co-culture (Figure 6J). In summary, endothelial inflammation during *in vivo* SARS-CoV-2 induction is most likely to occur in response to infection of the adjacent epithelial layer.

DISCUSSION

SARS-CoV-2 can induce vascular dysfunction and thrombotic events in patients with severe COVID-19. However, the cellular and molecular mechanisms by which SARS-CoV-2 infection triggers such pathologies have so far remained elusive. Here, we have shown that endothelial cells do not support productive replication of SARS-CoV-2, but that they induce pro-inflammatory cytokines and adhesion molecules upon either direct or indirect exposure to SARS-CoV-2 virions. This supports the hypothesis that the endothelial dysfunction observed in COVID-19 patients is likely to be largely mediated by inflammatory signalling pathways.

As COVID-19 case numbers rose, reports of COVID-19 coagulopathy and vascular dysfunction also began to accumulate. Whether SARS-CoV-2 directly infects the vasculature to drive this vascular pathology has thus remained a topic of intense debate. Multiple studies show viral particles surrounding the vasculature [3, 25, 43], yet it is unclear whether this infection is truly specific to the endothelium or occurs within the perivascular compartment. Our *in vivo* analyses of lung tissue samples from deceased COVID-19 patients indicates the endothelium often remains uninfected. Nevertheless, we showed that *in vitro,* endothelial cells are theoretically susceptible to SARS-CoV-2 infection, as they express ACE2, TMPRSS2 and NRP1, albeit at significantly lower levels than epithelial cells. This is in line with other studies that showed expression of SARS-CoV-2 receptors by the endothelium in human tissue or in cultured cells [14, 17, 23, 28]. However, we did not detect endothelial cell infection following exposure to 6 x 10^4 PFU of SARS-CoV-2, whereas epithelial cells were readily infected at the same viral dose. These results support those of Wang et al. [28], who showed that epithelial cells are more susceptible to infection than endothelial cells. When exposed to higher viral titres, endothelial cells were positive for viral NP protein, suggesting effective viral entry. However, no infectious virions were detected in the endothelial cell supernatant, indicating that this infection was abortive. It is interesting to speculate as to why SARS-CoV-2 infection is productive in a monoculture of epithelial, but not endothelial cells. This may relate to cell-dependent differences in viral entry. For example, in epithelial cells, there may be sufficient surface TMPRSS2 levels available to cleave the spike protein at the S2' site and mediate viral-host cell membrane fusion. This may in turn allow for efficient release of viral RNA into the cytoplasm and thus viral replication. In contrast, in cells with lower TMPRSS2 expression (such as endothelial cells), SARS-CoV-2 may enter the cell via endocytosis, with S2' cleavage being mediated by endosomal cathepsins [12]. Endosomal entry may not only be inefficient, but it may also activate the cellular anti-viral response and thereby limit productive viral replication [43, 44]. Alternatively, a host of other cellular co-factors expressed preferentially in epithelial cells may support selective SARS-CoV-2 replication, or endothelial-specific restriction factors may limit effective viral replication.

In contrast to endothelial cells in a monoculture, viral proteins could not be detected in endothelial cells grown in a co-culture with SARS-CoV-2-positive epithelial cells, despite being exposed to the same

high dose of virus. These data may reflect the fact that SARS-CoV-2 typically infects and buds from epithelial cells in an apical manner, resulting in limited exposure of the endothelium to infectious virions. Extrapolating these data to *in vivo* situation would suggest that a basolateral (abortive) infection of the endothelium by SARS-CoV-2 is only likely to occur when the epithelial barrier of the lung is severely damaged, exposing the endothelium to incoming virions.

While endothelial cells (either in a monoculture or in a co-culture) did not produce infectious virions, they did respond to SARS-CoV-2 infection. Analysis of infected endothelial monolayers revealed that cells positive for viral proteins were extruded in an apical fashion, without any apparent disruption to the monolayer, as assessed by phalloidin expression. This is in contrast to work from Buzhdygan and colleagues, who demonstrated that purified SARS-CoV-2 spike protein can induce the breakdown of the vascular barrier in brain microvascular endothelial cells [45]. Discrepancies between these results may be due to different sources of primary endothelial cells (lung versus brain), or the differences in response of the endothelium to a purified viral protein vs infectious virus [1, 3, 24, 26, 46-48]. However, if infected cells are promptly removed from exposed vessels as our data suggests, then this may explain why detection of viral particles in the endothelium of patients has varied between studies [4, 49].

In the absence of direct endothelial infection, hyperinflammation is likely to contribute to endothelial dysfunction observed in COVID-19 patients. SARS-CoV-2 triggered an upregulation of endothelial ICAM-1 expression when HMVEC-Ls were directly exposed to virus, or co-cultured with infected epithelial cells. ICAM-1 enables immune cells to effectively extravasate into tissues, so its upregulation is in keeping with the observed influx of inflammatory monocytes, neutrophils and other immune cells into the lungs in severe COVID-19 patients [50]. This suggests that locally produced pro-inflammatory cytokines stimulate the endothelium to induce adhesion marker expression. Our previous studies with influenza virus showed that endothelial cells can themselves be a source of these pro-inflammatory cytokines [51], and indeed we also observed SARS-CoV-2-induced release of IL-6 and CXCL10 in co-cultures. Precisely how SARS-CoV-2 is sensed by the endothelium in either the monoculture or co-culture system remains to be determined. Given that SARS-CoV-2 does not replicate in endothelial

cells, we speculate that endothelial cells are unlikely to sense this virus through cytosolic RNA receptors such as RIG-I or MDA5, as these immune sensors would detect viral replication intermediates. A more likely scenario is that the endothelial cells respond to danger signals from neighbouring infected epithelial or endothelial cells. These data add to a growing body of literature that indicate that endothelial cell-directed inflammation plays a key role in the pathogenesis of SARS-CoV-2 [52]. It is tempting to speculate that, similar to influenza virus, the SARS-CoV-2-induced pro-inflammatory state may induce endothelial cells to express tissue factor, which in turn induces a pro-coagulant state, microvascular leakage and pulmonary haemorrhage [53], all of which have been described in patients with severe COVID-19. Furthermore, regardless of direct or indirect infection, elevated IL-6 correlates with increased fibrinogen [54] and although still controversial, elevated fibrinogen levels have been detected in critically ill patients [2].

The present study was subject to several limitations. Firstly, coagulation, thrombosis and induction of angiogenesis in the lungs of deceased COVID-19 patients has been described in addition to endothelial dysfunction [3]. This angiogenic response is thought to be predominantly mediated through intussusceptive angiogenesis, where a new blood vessel is formed by splitting of an existing vessel. This effect appears to be specific to COVID-19 patients, as lungs from decreased influenza patients do not display increased angiogenic features. Whether this is due to relative hypoxia in the lungs remains unclear, although elevated angiogenic growth factors such as VEGF-A and VEGF-C have been associated with COVID-19 [3, 39]. In this study we have not addressed the effect of SARS-CoV-2 exposure on the angiogenic capacity of endothelial cells in culture. Given the intimate association between inflammation, endothelial dysfunction and angiogenesis [40, 55], these are critical aspects of COVID-19 pathology that remain to be addressed in subsequent studies.

An additional limitation of the present study is that, due to the reductionist nature of the *in vitro* systems used herein, we were unable to address the contribution of immune cells to endothelial cell dysfunction during SARS-CoV-2 infection. Multiple studies attribute the sustained inflammatory response directly to immune cells, wherein macrophage activation, monocyte NLRP3 inflammasome signalling,

complement activation and extrusion of neutrophil extracellular traps are implicated [41, 56-58]. Accordingly, our data may best reflect the initial stages of infection when only a limited number of tissue-resident leukocytes may be present. Future studies will necessitate the addition of leukocytes to our co-culture system, to determine whether their presence results in a further induction of inflammation and markers of severe disease.

Here, we have conclusively shown that *in vitro,* endothelial cells are not productively infected by SARS-CoV-2 but that they mount a robust inflammatory response after direct or indirect exposure to the virus, characterised by increased cytokine secretion and expression of adhesion molecules. Our results thus suggest a key role of the endothelium in the pathogenesis of COVID-19, and that targeting the inflammatory response may present the best opportunity to prevent endothelial dysfunction.

ACKNOWLEDGEMENTS AND FUNDING STATEMENT

This work is supported by the National Health and Medical Research Council of Australia (Fellowship 1141131 to KS, Project Grant APP1158002 to EG) and the Australian Research Council (Fellowship DE180100512 to KRS, Fellowship DE170100167 to EG, Discovery Project DP200100737 to EG and AL), and a UQ Early Career Researcher Grant (UQECR2058733 to LS).

CONFLICT STATEMENT

KS is a co-inventor on patent applications for NLRP3 inhibitors which have been licensed to Inflazome Ltd, a company headquartered in Dublin, Ireland. Inflazome is developing drugs that target the NLRP3 inflammasome to address unmet clinical needs in inflammatory disease. KS served on the Scientific Advisory Board of Inflazome in 2016–2017, and serves as a consultant to Quench Bio, USA and Novartis, Switzerland.

DATA AVAILABILITY STATEMENT

All raw data is available upon request.

FIGURE LEGENDS

Figure 1. In vivo sections of lung show endothelial cells are not infected. A) Lung tissue from a deceased COVID-19 patient was sectioned and stained for Hematoxylin and Eosin (H&E). Consecutive section was stained using RNAscope probes targeting SARS-CoV-2 spike mRNA and Syto13 for DNA. Enlargement of numbered insets show artery (1), vein (2) and venule (3) outlined with red dashed line are negative for SARS-CoV-2 spike mRNA in the endothelial layer of the vessels.

Figure 2. Endothelial cells express very low levels of ACE2 and TMPRSS2 receptors. A) qPCR shows presence of mRNA for ACE2, TMPRSS2 and NRP1 in HUVEC, HMVEC-L and Calu-3 cells. n=3 independent experiments. **B)** Western blot analysis showing ACE2 and TMPRSS2 protein levels are lower in HUVEC and HMVEC-L compared to Calu-3 cells. **C)** Quantification of protein levels for ACE2 and TMPRSS2 in HUVEC, HMVEC-L and Calu-3. n=4 (HUVEC and HMVEC-L), n=2 (Calu-3) independent experiments. **D)** Representative immunofluorescent images of HUVEC, HMVEC-L and Calu-3 cells stained for ACE2 (shown as single channel in top panel) (green), Phalloidin (magenta) and DAPI (blue). Scalebar 30 µm. **E)** Quantification of ACE2 staining intensity. n=15 images from 3 independent experiments. Data are presented as mean±s.e.m. with individual data points indicated and colour coded per independent experimental replicate. Statistical significance was determined using a Kruskal Wallis test between Calu-3 and all others (A, C, E). *P<0.05, ****P<0.0001.

Figure 3. Endothelial cells are not productively infected with 6 x 10^4 PFU of SARS-CoV-2. Schematic of **A)** apical and **B)** basolateral infection of cells cultured on transwell membranes. **C)** Viral replication shown as number of PFU per ml of supernatant from SARS-CoV-2 infected HUVEC, HMVEC-L and Calu-3 cells at 24h, 48h and 72h after infection. n=2 (HUVEC and HMVEC-L), n=3 (Calu-3) independent experiments. Representative immunofluorescent images of **D)** HUVEC, **E)** Calu-3 or **F)** HMVEC-L stained for NP (shown as single channel in top panel) (green), phalloidin (magenta) and DAPI (blue) with mock or SARS-CoV-2 infection from either apical or basolateral side of the cells at 48h after infection. Scalebar 50 µm. **G)** Quantification of NP staining intensity in HUVEC, HMVEC-L and Calu-3. n=9 images from 3 independent experiments. **H)** Western blot analysis showing NP

protein levels in HUVEC, HMVEC-L and Calu-3 cells after 48h of infection. **I)** Quantification of protein levels for NP in HUVEC, HMVEC-L and Calu-3. n=2 independent experiments. Data are presented as mean±s.e.m. with individual data points indicated and colour coded per independent experimental replicate. Statistical significance was determined using Kruskal Wallis test between 24h and other time points (C) or Mann-Whitney test between mock and + SARS-CoV-2 (G, I). *P<0.05, **P<0.01

Figure 4. Endothelial cells can be infected with 2 x 10^6 PFU of SARS-CoV-2, but infection is abortive. **A)** Viral replication shown as number of PFU per ml of supernatant from SARS-CoV-2 infected HUVEC, HMVEC-L and Calu-3 cells at 24h, 48h and 72h after infection. n=2 (HUVEC and HMVEC-L), n=3 (Calu-3) independent experiments. **B)** Representative immunofluorescent images of HMVEC-L stained for NP (shown as single channel in top panel) (green), phalloidin (magenta) and DAPI (blue) with mock or SARS-CoV-2 infection from either apical or basolateral side of the cells at 72h after infection. Scalebar 50 µm. **B')** Enlargement of white box in B shows Phalloidin and DAPI single channels and merge. Scalebar 10 µm. **B'')** XZ projection of merged image in B', with apical side on top of image and basolateral side on the bottom. Scalebar 10 µm. **C)** Quantification of NP staining intensity in HMVEC-L. n=15 images from 3 independent experiments. **D)** Western blot analysis showing NP and ORF7a protein levels in HUVEC, HMVEC-L and Calu-3 cells after 72h of infection. Quantification of **E)** NP protein levels and **F)** ORF7a protein levels in HUVEC, HMVEC-L and Calu-3. n=3 (NP), n=2(ORF7a) independent experiments. Data are presented as mean±s.e.m. with individual data points indicated and colour coded per independent experimental replicate. Statistical significance was determined using Kruskal Wallis test between 24h and other time points (A) or Mann-Whitney test between mock and + SARS-CoV-2 (C, E, F). *P<0.05, ***P<0.001, ****P<0.0001.

Figure 5. Endothelial cells mount an inflammatory response upon infection. Representative immunofluorescent images of HMVEC-L stained for ICAM-1 (shown as single channel in top panel) (green), NP (magenta), phalloidin (grey) and DAPI (blue) with **A)** mock or SARS-CoV-2 infection from either apical or basolateral side of the cells at 72h after infection or with **B)** control and TNFα

treatment for 16h. Scalebar 50 µm. **C)** Quantification of ICAM-1 staining intensity in HMVEC-L. n=15 images from 3 independent experiments. **D)** Western blot analysis showing ICAM-1 and NP protein levels in HMVEC-L and Calu-3 cells after 72h of infection. **E)** Quantification of ICAM-1 protein levels in HMVEC-L and Calu-3. n=3 independent experiments. Measurement of cytokines with AlphaLISA Immunoassay kit for **F)** CXCL10 and **G)** IL6 in the supernatant of HMVEC-L with mock or SARS-CoV-2 infection from either apical or basolateral side of the cells at 72h after infection. n=4 independent experiments. Data are presented as mean±s.e.m. with individual data points indicated and colour coded per independent experimental replicate. Statistical significance was determined using Mann-Whitney test between mock and + SARS-CoV-2 (C, E, F, G). *P<0.05, ****P<0.0001.

Figure 6. Co-culture shows infection of Calu-3 and inflammation of HMVEC-L. A) Representative immunofluorescent images of co-cultured Calu-3 and HMVEC-L stained for NP (shown as single channel in top panel) (magenta), ICAM-1 (shown as single channel in middle panel) (green), phalloidin (grey) and DAPI (blue) with mock or SARS-CoV-2 infection at 72h after infection. Scalebar 50 µm. **B)** Quantification of NP staining intensity in Calu-3 and HMVEC-L. n=9 images from 3 independent experiments. **C)** Schematic of Calu-3 and HMVEC-L co-cultures on transwell membranes. **D)** Quantification of ICAM-1 staining intensity in Calu-3 and HMVEC-L. n=9 images from 3 independent experiments. **E)** Representative immunofluorescent images of co-cultured Calu-3 and HMVEC-L stained for dsRNA (shown as single channel in top panel) (magenta), phalloidin (grey) and DAPI (blue) with mock or SARS-CoV-2 infection at 72h after infection. Scalebar 50 µm. **F)** Quantification of dsRNA staining intensity in Calu-3 and HMVEC-L. n=9 images from 3 independent experiments. **G)** qPCR shows presence of viral RNA (MPRO) in SARS-CoV-2 infected Calu-3 and HMVEC-L co-cultured cells represented as fold change relative to mock infection at 72h after infection. n=3 independent experiments. **H)** Viral replication shown as number of PFU per ml of supernatant from SARS-CoV-2 infected Calu-3 and HMVEC-L co-cultured cells at 72h after infection. n=3 independent experiments. Measurement of cytokines with AlphaLISA Immunoassay kit for **I)** CXCL10 and **J)** IL6 in the supernatant of Calu-3 and HMVEC-L co-cultured cells with mock or SARS-CoV-2 infection at 72h after infection. n=4 independent experiments. Data are presented as mean±s.e.m. with individual

data points indicated and colour coded per independent experimental replicate. Statistical significance was determined using Mann-Whitney test between mock and + SARS-CoV-2 (B, D, F, G, H, I, J). *P<0.05, **P<0.01, ****P<0.0001.

Supplemental Figure 1. Viral RNA levels in monocultures. A) qPCR analysis shows presence of viral RNA (MRPO) in SARS-CoV-2 infected HUVEC, HMVEC-L and Calu-3 represented as fold change relative to mock infection at 48h after infection with 6 x 10^4 PFU. n=4 independent experiments. **B)** qPCR shows presence of viral RNA (MPRO) in SARS-CoV-2 infected HUVEC, HMVEC-L and Calu-3 represented as fold change relative to mock infection at 72h after infection with 2 x 10^6 PFU. n=3 independent experiments. **C)** Quantification of % NP positive cells that are extruded upon SARS-CoV-2 infection of HMVEC-Ls. n=15 images from 3 independent experiments. Data are presented as mean±s.e.m. with individual data points indicated and colour coded per independent experimental replicate. Statistical significance was determined using Kruskal Wallis test between Calu-3 and all others (A, B). *P<0.05.

REFERENCES

1. Teuwen LA, Geldhof V, Pasut A, Carmeliet P. COVID-19: the vasculature unleashed. Nat Rev Immunol. 2020;20(7):389-91. Epub 2020/05/23. doi: 10.1038/s41577-020-0343-0. PubMed PMID: 32439870; PubMed Central PMCID: PMCPMC7240244.

2. Gu SX, Tyagi T, Jain K, Gu VW, Lee SH, Hwa JM, et al. Thrombocytopathy and endotheliopathy: crucial contributors to COVID-19 thromboinflammation. Nature Reviews Cardiology. 2020. doi: 10.1038/s41569-020-00469-1.

3. Ackermann M, Verleden SE, Kuehnel M, Haverich A, Welte T, Laenger F, et al. Pulmonary Vascular Endothelialitis, Thrombosis, and Angiogenesis in Covid-19. N Engl J Med. 2020;383(2):120-8. Epub 2020/05/22. doi: 10.1056/NEJMoa2015432. PubMed PMID: 32437596; PubMed Central PMCID: PMCPMC7412750.

4. Goshua G, Pine AB, Meizlish ML, Chang CH, Zhang H, Bahel P, et al. Endotheliopathy in COVID-19-associated coagulopathy: evidence from a single-centre, cross-sectional study. Lancet

Haematol. 2020;7(8):e575-e82. Epub 2020/07/04. doi: 10.1016/S2352-3026(20)30216-7. PubMed PMID: 32619411; PubMed Central PMCID: PMCPMC7326446.

5. Sardu C, Gambardella J, Morelli MB, Wang X, Marfella R, Santulli G. Hypertension, Thrombosis, Kidney Failure, and Diabetes: Is COVID-19 an Endothelial Disease? A Comprehensive Evaluation of Clinical and Basic Evidence. J Clin Med. 2020;9(5). Epub 2020/05/15. doi: 10.3390/jcm9051417. PubMed PMID: 32403217; PubMed Central PMCID: PMCPMC7290769.

6. Gupta A, Madhavan MV, Sehgal K, Nair N, Mahajan S, Sehrawat TS, et al. Extrapulmonary manifestations of COVID-19. Nature medicine. 2020;26(7):1017-32. Epub 2020/07/12. doi: 10.1038/s41591-020-0968-3. PubMed PMID: 32651579.

7. Cantuti-Castelvetri L, Ojha R, Pedro LD, Djannatian M, Franz J, Kuivanen S, et al. Neuropilin-1 facilitates SARS-CoV-2 cell entry and infectivity. Science. 2020. Epub 2020/10/22. doi: 10.1126/science.abd2985. PubMed PMID: 33082293.

8. Daly JL, Simonetti B, Klein K, Chen KE, Williamson MK, Antón-Plágaro C, et al. Neuropilin-1 is a host factor for SARS-CoV-2 infection. Science. 2020. Epub 2020/10/22. doi: 10.1126/science.abd3072. PubMed PMID: 33082294.

9. Zhou P, Yang X-L, Wang X-G, Hu B, Zhang L, Zhang W, et al. A pneumonia outbreak associated with a new coronavirus of probable bat origin. Nature. 2020;579(7798):270-3. doi: 10.1038/s41586-020-2012-7.

10. Matheson NJ, Lehner PJ. How does SARS-CoV-2 cause COVID-19? Science. 2020;369(6503):510-1. Epub 2020/08/01. doi: 10.1126/science.abc6156. PubMed PMID: 32732413.

11. Hoffmann M, Kleine-Weber H, Schroeder S, Krüger N, Herrler T, Erichsen S, et al. SARS-CoV-2 Cell Entry Depends on ACE2 and TMPRSS2 and Is Blocked by a Clinically Proven Protease Inhibitor. Cell. 2020;181(2):271-80.e8. Epub 2020/03/07. doi: 10.1016/j.cell.2020.02.052. PubMed PMID: 32142651; PubMed Central PMCID: PMCPMC7102627.

12. Laporte M, Stevaert A, Raeymaekers V, Van Berwaer R, Martens K, Pöhlmann S, et al. The SARS-CoV-2 and other human coronavirus spike proteins are fine-tuned towards temperature and proteases of the human airways. bioRxiv. 2020:2020.11.09.374603. doi: 10.1101/2020.11.09.374603.

13. Ferrario CM, Jessup J, Chappell MC, Averill DB, Brosnihan KB, Tallant EA, et al. Effect of angiotensin-converting enzyme inhibition and angiotensin II receptor blockers on cardiac angiotensin-converting enzyme 2. Circulation. 2005;111(20):2605-10. Epub 2005/05/18. doi: 10.1161/circulationaha.104.510461. PubMed PMID: 15897343.

14. Nicin L, Abplanalp WT, Mellentin H, Kattih B, Tombor L, John D, et al. Cell type-specific expression of the putative SARS-CoV-2 receptor ACE2 in human hearts. Eur Heart J. 2020;41(19):1804-6. Epub 2020/04/16. doi: 10.1093/eurheartj/ehaa311. PubMed PMID: 32293672; PubMed Central PMCID: PMCPMC7184464.

15. Sluimer JC, Gasc JM, Hamming I, van Goor H, Michaud A, van den Akker LH, et al. Angiotensin-converting enzyme 2 (ACE2) expression and activity in human carotid atherosclerotic lesions. J Pathol. 2008;215(3):273-9. Epub 2008/05/24. doi: 10.1002/path.2357. PubMed PMID: 18498093.

16. Lu R, Zhao X, Li J, Niu P, Yang B, Wu H, et al. Genomic characterisation and epidemiology of 2019 novel coronavirus: implications for virus origins and receptor binding. Lancet. 2020;395(10224):565-74. Epub 2020/02/03. doi: 10.1016/s0140-6736(20)30251-8. PubMed PMID: 32007145; PubMed Central PMCID: PMCPMC7159086.

17. Hikmet F, Méar L, Edvinsson Å, Micke P, Uhlén M, Lindskog C. The protein expression profile of ACE2 in human tissues. Molecular Systems Biology. 2020;16(7):e9610. doi: https://doi.org/10.15252/msb.20209610.

18. Soker S, Takashima S, Miao HQ, Neufeld G, Klagsbrun M. Neuropilin-1 is expressed by endothelial and tumor cells as an isoform-specific receptor for vascular endothelial growth factor. Cell. 1998;92(6):735-45. Epub 1998/04/07. doi: 10.1016/s0092-8674(00)81402-6. PubMed PMID: 9529250.

19. Kitsukawa T, Shimono A, Kawakami A, Kondoh H, Fujisawa H. Overexpression of a membrane protein, neuropilin, in chimeric mice causes anomalies in the cardiovascular system, nervous system and limbs. Development. 1995;121(12):4309-18. Epub 1995/12/01. PubMed PMID: 8575331.

20. Gerhardt H, Ruhrberg C, Abramsson A, Fujisawa H, Shima D, Betsholtz C. Neuropilin-1 is required for endothelial tip cell guidance in the developing central nervous system. Developmental

dynamics : an official publication of the American Association of Anatomists. 2004;231(3):503-9. Epub 2004/09/18. doi: 10.1002/dvdy.20148. PubMed PMID: 15376331.

21. Jones EA, Yuan L, Breant C, Watts RJ, Eichmann A. Separating genetic and hemodynamic defects in neuropilin 1 knockout embryos. Development. 2008;135(14):2479-88. Epub 2008/06/14. doi: 10.1242/dev.014902. PubMed PMID: 18550715.

22. Aspalter IM, Gordon E, Dubrac A, Ragab A, Narloch J, Vizan P, et al. Alk1 and Alk5 inhibition by Nrp1 controls vascular sprouting downstream of Notch. Nature communications. 2015;6. doi: 10.1038/ncomms8264. PubMed PMID: WOS:000357170300001.

23. Aimes RT, Zijlstra A, Hooper JD, Ogbourne SM, Sit ML, Fuchs S, et al. Endothelial cell serine proteases expressed during vascular morphogenesis and angiogenesis. Thromb Haemost. 2003;89(3):561-72. Epub 2003/03/08. PubMed PMID: 12624642.

24. Chen L, Li X, Chen M, Feng Y, Xiong C. The ACE2 expression in human heart indicates new potential mechanism of heart injury among patients infected with SARS-CoV-2. Cardiovascular research. 2020;116(6):1097-100. Epub 2020/04/01. doi: 10.1093/cvr/cvaa078. PubMed PMID: 32227090; PubMed Central PMCID: PMCPMC7184507.

25. Schaefer I-M, Padera RF, Solomon IH, Kanjilal S, Hammer MM, Hornick JL, et al. In situ detection of SARS-CoV-2 in lungs and airways of patients with COVID-19. Modern Pathology. 2020;33(11):2104-14. doi: 10.1038/s41379-020-0595-z.

26. Varga Z, Flammer AJ, Steiger P, Haberecker M, Andermatt R, Zinkernagel AS, et al. Endothelial cell infection and endotheliitis in COVID-19. Lancet. 2020;395(10234):1417-8. Epub 2020/04/24. doi: 10.1016/S0140-6736(20)30937-5. PubMed PMID: 32325026; PubMed Central PMCID: PMCPMC7172722.

27. Amraie R, Napoleon MA, Yin W, Berrigan J, Suder E, Zhao G, et al. CD209L/L-SIGN and CD209/DC-SIGN act as receptors for SARS-CoV-2 and are differentially expressed in lung and kidney epithelial and endothelial cells. bioRxiv. 2020:2020.06.22.165803. doi: 10.1101/2020.06.22.165803. PubMed PMID: 32607506.

28. Wang P, Luo R, Zhang M, Wang Y, Song T, Tao T, et al. A cross-talk between epithelium and endothelium mediates human alveolar–capillary injury during SARS-CoV-2 infection. Cell Death & Disease. 2020;11(12):1042. doi: 10.1038/s41419-020-03252-9.

29. Monteil V, Kwon H, Prado P, Hagelkrüys A, Wimmer RA, Stahl M, et al. Inhibition of SARS-CoV-2 Infections in Engineered Human Tissues Using Clinical-Grade Soluble Human ACE2. Cell. 2020;181(4):905-13.e7. Epub 2020/04/24. doi: 10.1016/j.cell.2020.04.004. PubMed PMID: 32333836.

30. Bryce C, Grimes Z, Pujadas E, Ahuja S, Beasley MB, Albrecht R, et al. Pathophysiology of SARS-CoV-2: targeting of endothelial cells renders a complex disease with thrombotic microangiopathy and aberrant immune response. The Mount Sinai COVID-19 autopsy experience. medRxiv. 2020:2020.05.18.20099960. doi: 10.1101/2020.05.18.20099960.

31. Ko CJ, Harigopal M, Gehlhausen JR, Bosenberg M, McNiff JM, Damsky W. Discordant anti-SARS-CoV-2 spike protein and RNA staining in cutaneous perniotic lesions suggests endothelial deposition of cleaved spike protein. Journal of Cutaneous Pathology. n/a(n/a). doi: 10.1111/cup.13866.

32. Baeck M, Hoton D, Marot L, Herman A. Chilblains and COVID-19: why SARS-CoV-2 endothelial infection is questioned. British Journal of Dermatology. n/a(n/a). doi: 10.1111/bjd.19489.

33. Sia SF, Yan L-M, Chin AWH, Fung K, Choy K-T, Wong AYL, et al. Pathogenesis and transmission of SARS-CoV-2 in golden hamsters. Nature. 2020;583(7818):834-8. doi: 10.1038/s41586-020-2342-5.

34. Rockx B, Kuiken T, Herfst S, Bestebroer T, Lamers MM, Oude Munnink BB, et al. Comparative pathogenesis of COVID-19, MERS, and SARS in a nonhuman primate model. Science. 2020;368(6494):1012-5. doi: 10.1126/science.abb7314.

35. Aid M, Busman-Sahay K, Vidal SJ, Maliga Z, Bondoc S, Starke C, et al. Vascular Disease and Thrombosis in SARS-CoV-2-Infected Rhesus Macaques. Cell. 2020;183(5):1354-66.e13. Epub 2020/10/17. doi: 10.1016/j.cell.2020.10.005. PubMed PMID: 33065030; PubMed Central PMCID: PMCPMC7546181.

36. Milewska A, Kula-Pacurar A, Wadas J, Suder A, Szczepanski A, Dabrowska A, et al. Replication of Severe Acute Respiratory Syndrome Coronavirus 2 in Human Respiratory Epithelium. Journal of Virology. 2020;94(15):e00957-20. doi: 10.1128/jvi.00957-20.

37. Andersson MI, Arancibia-Carcamo CV, Auckland K, Baillie JK, Barnes E, Beneke T, et al. SARS-CoV-2 RNA detected in blood products from patients with COVID-19 is not associated with infectious virus. Wellcome Open Res. 2020;5:181. Epub 2020/12/09. doi: 10.12688/wellcomeopenres.16002.2. PubMed PMID: 33283055; PubMed Central PMCID: PMCPMC7689603.

38. Gordon DE, Jang GM, Bouhaddou M, Xu J, Obernier K, White KM, et al. A SARS-CoV-2 protein interaction map reveals targets for drug repurposing. Nature. 2020;583(7816):459-68. doi: 10.1038/s41586-020-2286-9.

39. Lucas C, Wong P, Klein J, Castro TBR, Silva J, Sundaram M, et al. Longitudinal analyses reveal immunological misfiring in severe COVID-19. Nature. 2020;584(7821):463-9. doi: 10.1038/s41586-020-2588-y.

40. Pober JS, Sessa WC. Evolving functions of endothelial cells in inflammation. Nat Rev Immunol. 2007;7(10):803-15. Epub 2007/09/26. doi: 10.1038/nri2171. PubMed PMID: 17893694.

41. Rodrigues TS, de Sá KSG, Ishimoto AY, Becerra A, Oliveira S, Almeida L, et al. Inflammasomes are activated in response to SARS-CoV-2 infection and are associated with COVID-19 severity in patients. Journal of Experimental Medicine. 2020;218(3). doi: 10.1084/jem.20201707.

42. Kasper J, Hermanns MI, Bantz C, Maskos M, Stauber R, Pohl C, et al. Inflammatory and cytotoxic responses of an alveolar-capillary coculture model to silica nanoparticles: Comparison with conventional monocultures. Particle and Fibre Toxicology. 2011;8(1):6. doi: 10.1186/1743-8977-8-6.

43. Kummer S, Avinoam O, Kräusslich H-G. IFITM3 Clusters on Virus Containing Endosomes and Lysosomes Early in the Influenza A Infection of Human Airway Epithelial Cells. Viruses. 2019;11(6):548. doi: 10.3390/v11060548. PubMed PMID: 31212878.

44. Winstone H, Lista MJ, Reid A, Pickering S, Doores KJ, Swanson C, et al. The polybasic cleavage site in the SARS-CoV-2 spike modulates viral sensitivity to Type I IFN and IFITM2. bioRxiv. 2020:2020.12.19.423592. doi: 10.1101/2020.12.19.423592.

45. Buzhdygan TP, DeOre BJ, Baldwin-Leclair A, McGary H, Razmpour R, Galie PA, et al. The SARS-CoV-2 spike protein alters barrier function in 2D static and 3D microfluidic in vitro models of

the human blood-brain barrier. bioRxiv. 2020:2020.06.15.150912. doi: 10.1101/2020.06.15.150912. PubMed PMID: 32587958.

46. Bradley BT, Maioli H, Johnston R, Chaudhry I, Fink SL, Xu H, et al. Histopathology and ultrastructural findings of fatal COVID-19 infections in Washington State: a case series. Lancet. 2020;396(10247):320-32. Epub 2020/07/20. doi: 10.1016/s0140-6736(20)31305-2. PubMed PMID: 32682491; PubMed Central PMCID: PMCPMC7365650.

47. Manne BK, Denorme F, Middleton EA, Portier I, Rowley JW, Stubben C, et al. Platelet gene expression and function in patients with COVID-19. Blood. 2020;136(11):1317-29. Epub 2020/06/24. doi: 10.1182/blood.2020007214. PubMed PMID: 32573711; PubMed Central PMCID: PMCPMC7483430.

48. Schurink B, Roos E, Radonic T, Barbe E, Bouman CSC, de Boer HH, et al. Viral presence and immunopathology in patients with lethal COVID-19: a prospective autopsy cohort study. Lancet Microbe. 2020;1(7):e290-e9. Epub 2020/10/06. doi: 10.1016/s2666-5247(20)30144-0. PubMed PMID: 33015653; PubMed Central PMCID: PMCPMC7518879.

49. Meizlish M, Pine A, Goshua G, Chang C-H, Zhang H, Bishai J, et al. Circulating Markers of Angiogenesis and Endotheliopathy in COVID-19. medRxiv. 2020:2020.06.29.20140376. doi: 10.1101/2020.06.29.20140376.

50. Bost P, Giladi A, Liu Y, Bendjelal Y, Xu G, David E, et al. Host-Viral Infection Maps Reveal Signatures of Severe COVID-19 Patients. Cell. 2020;181(7):1475-88.e12. Epub 2020/05/08. doi: 10.1016/j.cell.2020.05.006. PubMed PMID: 32479746.

51. Short KR, Kasper J, van der Aa S, Andeweg AC, Zaaraoui-Boutahar F, Goeijenbier M, et al. Influenza virus damages the alveolar barrier by disrupting epithelial cell tight junctions. Eur Respir J. 2016;47(3):954-66. Epub 2016/01/09. doi: 10.1183/13993003.01282-2015. PubMed PMID: 26743480.

52. Bernard I, Limonta D, Mahal LK, Hobman TC. Endothelium Infection and Dysregulation by SARS-CoV-2: Evidence and Caveats in COVID-19. Viruses. 2020;13(1). Epub 2020/12/31. doi: 10.3390/v13010029. PubMed PMID: 33375371.

53. Goeijenbier M, van Gorp ECM, Van den Brand JMA, Stittelaar K, Bakhtiari K, Roelofs JJTH, et al. Activation of coagulation and tissue fibrin deposition in experimental influenza in ferrets. BMC Microbiology. 2014;14(1):134. doi: 10.1186/1471-2180-14-134.

54. Ranucci M, Ballotta A, Di Dedda U, Bayshnikova E, Dei Poli M, Resta M, et al. The procoagulant pattern of patients with COVID-19 acute respiratory distress syndrome. J Thromb Haemost. 2020;18(7):1747-51. Epub 2020/04/18. doi: 10.1111/jth.14854. PubMed PMID: 32302448.

55. McDonald DM, Yao LC, Baluk P. Dynamics of airway blood vessels and lymphatics: lessons from development and inflammation. Proc Am Thorac Soc. 2011;8(6):504-7. doi: 10.1513/pats.201102-022MW. PubMed PMID: 22052927; PubMed Central PMCID: PMCPMC3359074.

56. Merad M, Martin JC. Pathological inflammation in patients with COVID-19: a key role for monocytes and macrophages. Nat Rev Immunol. 2020;20(6):355-62. Epub 2020/05/08. doi: 10.1038/s41577-020-0331-4. PubMed PMID: 32376901; PubMed Central PMCID: PMCPMC7201395.

57. Middleton EA, He XY, Denorme F, Campbell RA, Ng D, Salvatore SP, et al. Neutrophil extracellular traps contribute to immunothrombosis in COVID-19 acute respiratory distress syndrome. Blood. 2020;136(10):1169-79. Epub 2020/07/01. doi: 10.1182/blood.2020007008.

58. Zuo Y, Yalavarthi S, Shi H, Gockman K, Zuo M, Madison JA, et al. Neutrophil extracellular traps in COVID-19. JCI Insight. 2020;5(11). Epub 2020/04/25. doi: 10.1172/jci.insight.138999. PubMed PMID: 32329756; PubMed Central PMCID: PMCPMC7308057.

Figure 1

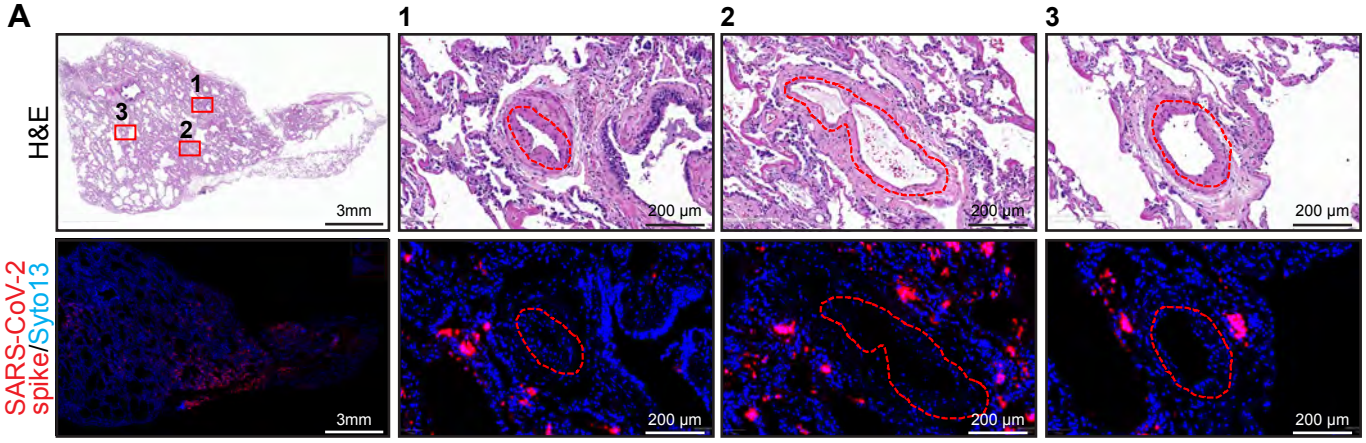

Figure 2

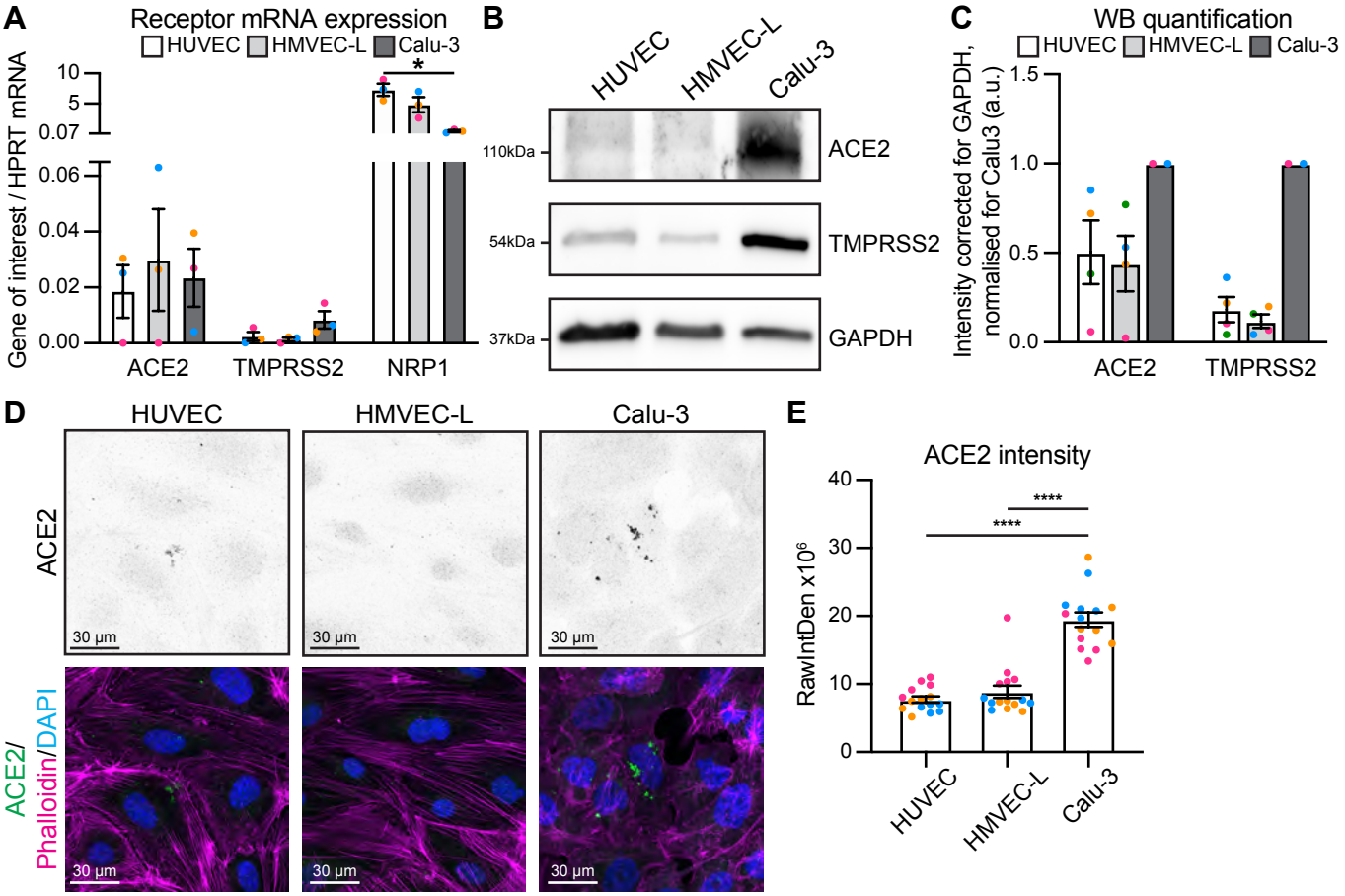
A
Receptor mRNA expression
HUVEC
HMVEC-L
Calu-3
Gene of interest / HPRT mRNA
10
5
0.07
0.06
0.04
0.02
0.00
*
ACE2
TMPRSS2
NRP1
B
HUVEC
HMVEC-L
Calu-3
110kDa
ACE2
54kDa
TMPRSS2
37kDa
GAPDH
C
WB quantification
HUVEC
HMVEC-L
Calu-3
Intensity corrected for GAPDH, normalised for Calu3 (a.u.)
1.5
1.0
0.5
0.0
ACE2
TMPRSS2
D
HUVEC
HMVEC-L
Calu-3
ACE2
30 µm
ACE2/
Phalloidin/DAPI
E
ACE2 intensity
RawIntDen x10⁶
40
30
20
10
0
****
****
HUVEC
HMVEC-L
Calu-3

Figure 3

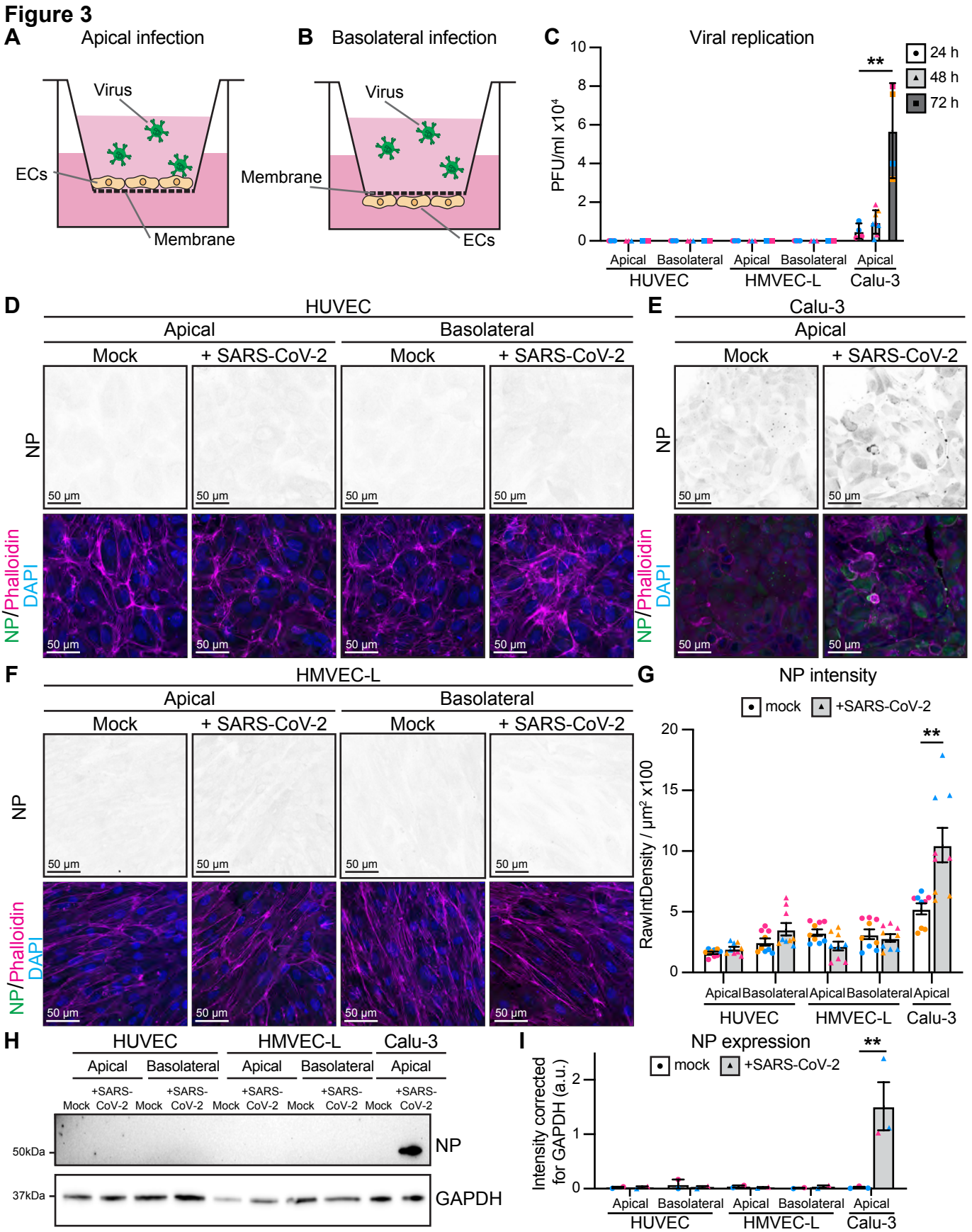
A
Apical infection
Virus
ECs
Membrane
B
Basolateral infection
Virus
Membrane
ECs
C
Viral replication
PFU/ml x10⁴
24 h
48 h
72 h
**
Apical
Basolateral
Apical
Basolateral
Apical
HUVEC
HMVEC-L
Calu-3
D
HUVEC
Apical
Basolateral
Mock
+ SARS-CoV-2
Mock
+ SARS-CoV-2
NP
NP/Phalloidin
DAPI
50 µm
E
Calu-3
Apical
Mock
+ SARS-CoV-2
NP
NP/Phalloidin
DAPI
50 µm
F
HMVEC-L
Apical
Basolateral
Mock
+ SARS-CoV-2
Mock
+ SARS-CoV-2
NP
NP/Phalloidin
DAPI
50 µm
G
NP intensity
mock
+SARS-CoV-2
**
RawIntDensity / µm² x100
Apical
Basolateral
Apical
Basolateral
Apical
HUVEC
HMVEC-L
Calu-3
H
HUVEC
HMVEC-L
Calu-3
Apical
Basolateral
Apical
Basolateral
Apical
Mock
+SARS-CoV-2
Mock
+SARS-CoV-2
Mock
+SARS-CoV-2
Mock
+SARS-CoV-2
Mock
+SARS-CoV-2
50kDa
NP
37kDa
GAPDH
I
NP expression
mock
+SARS-CoV-2
**
Intensity corrected for GAPDH (a.u.)
Apical
Basolateral
Apical
Basolateral
Apical
HUVEC
HMVEC-L
Calu-3

Figure 4

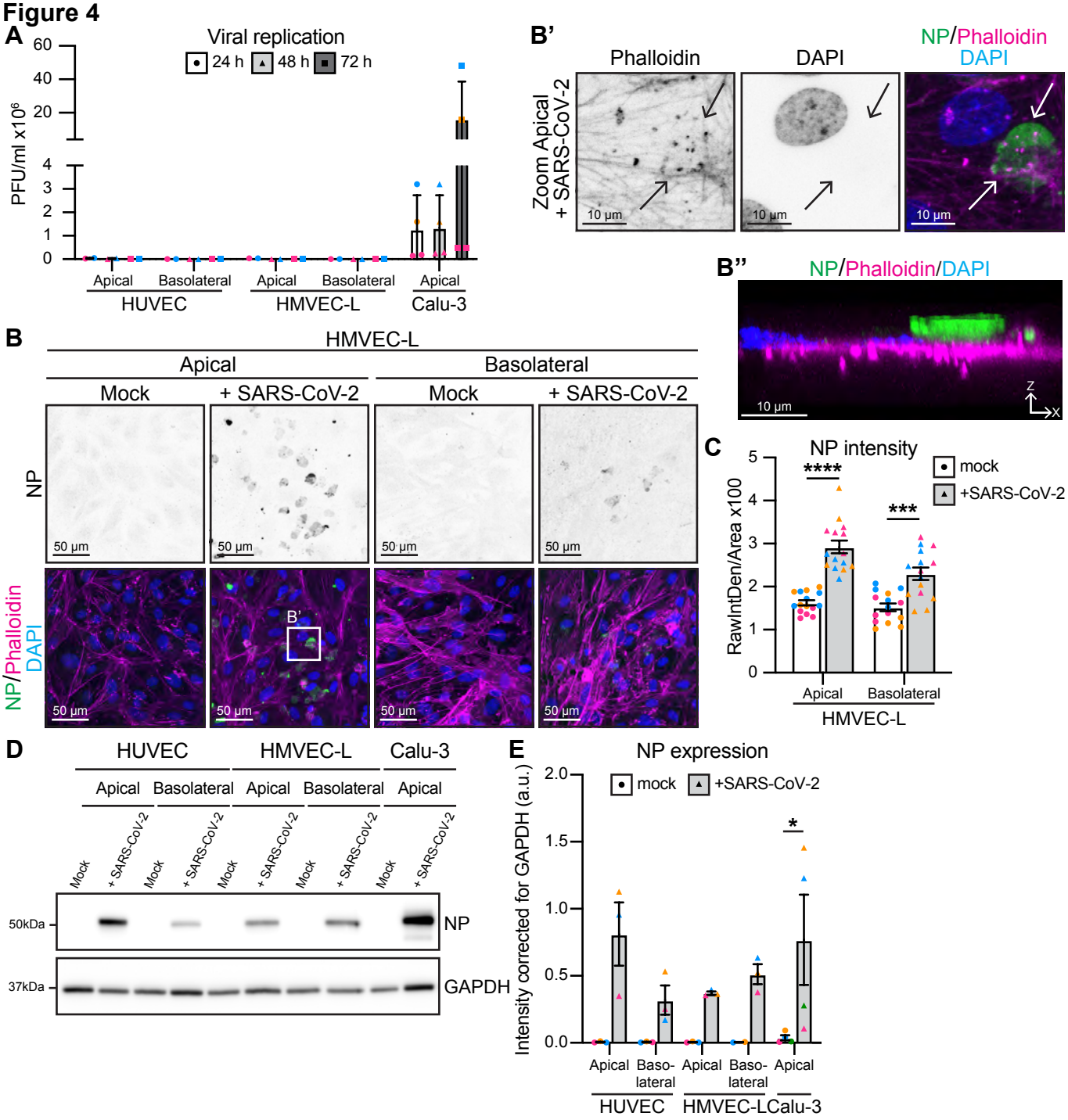
A
Viral replication
24 h
48 h
72 h
PFU/ml x10^6
60
40
20
4
3
2
1
0
Apical
Basolateral
Apical
Basolateral
Apical
HUVEC
HMVEC-L
Calu-3
B'
Phalloidin
DAPI
NP/Phalloidin
DAPI
Zoom Apical
+ SARS-CoV-2
10 µm
B''
NP/Phalloidin/DAPI
10 µm
Z
X
B
HMVEC-L
Apical
Basolateral
Mock
+ SARS-CoV-2
Mock
+ SARS-CoV-2
NP
NP/Phalloidin
DAPI
50 µm
B'
C
NP intensity
mock
+SARS-CoV-2
RawIntDen/Area x100
****
***
Apical
Basolateral
HMVEC-L
D
HUVEC
HMVEC-L
Calu-3
Apical
Basolateral
Apical
Basolateral
Apical
Mock
+ SARS-CoV-2
50kDa
37kDa
NP
GAPDH
E
NP expression
mock
+SARS-CoV-2
Intensity corrected for GAPDH (a.u.)
2.0
1.5
1.0
0.5
0.0
*
Apical
Baso-
lateral
Apical
Baso-
lateral
Apical
HUVEC
HMVEC-L
Calu-3

Figure 5

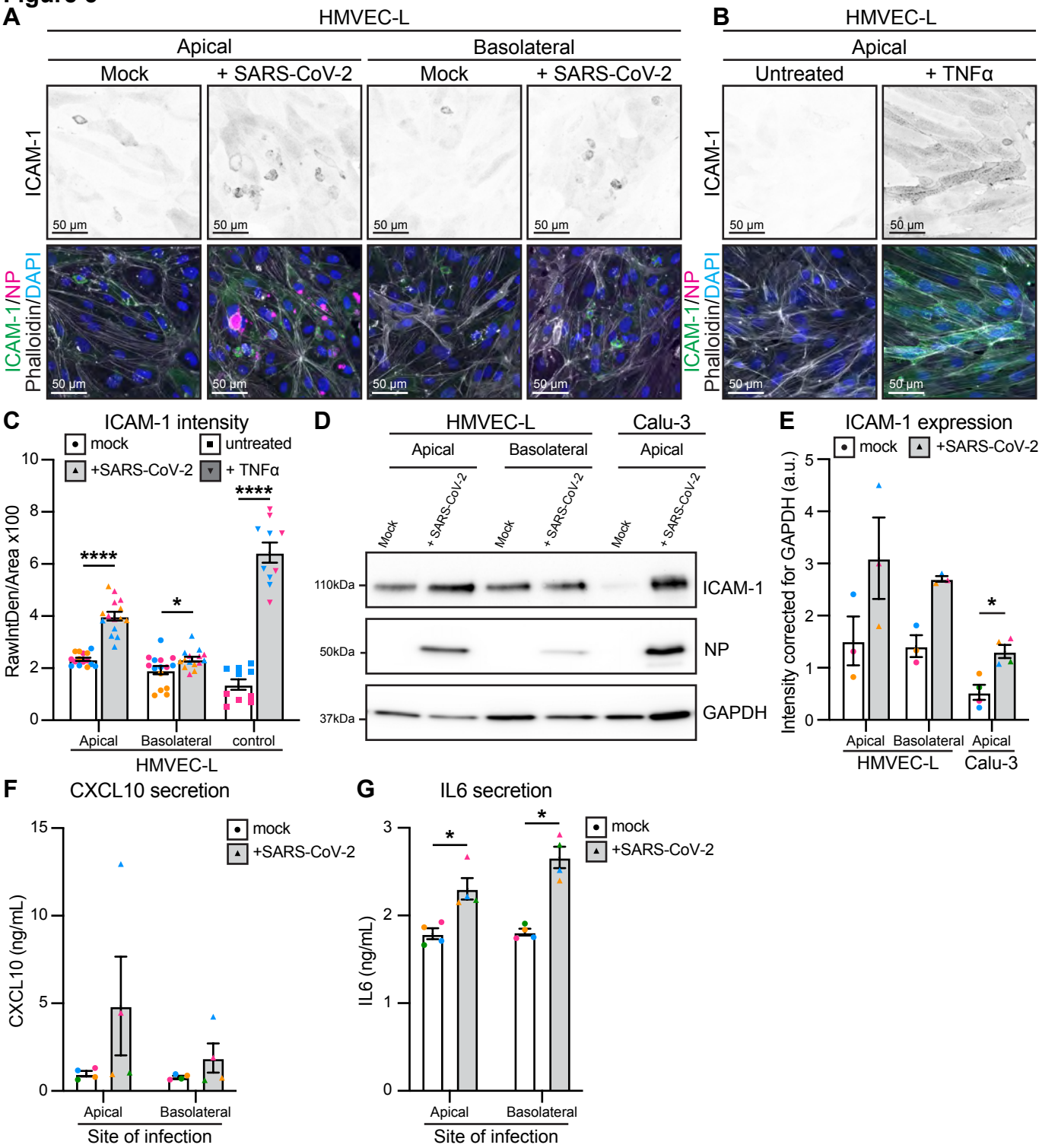
A
HMVEC-L
Apical
Basolateral
Mock
+ SARS-CoV-2
Mock
+ SARS-CoV-2
ICAM-1
ICAM-1/NP
Phalloidin/DAPI
50 µm
B
HMVEC-L
Apical
Untreated
+ TNFα
ICAM-1
ICAM-1/NP
Phalloidin/DAPI
50 µm
C
ICAM-1 intensity
mock
untreated
+SARS-CoV-2
+ TNFα
RawIntDen/Area x100
****
*
****
Apical
Basolateral
control
HMVEC-L
D
HMVEC-L
Calu-3
Apical
Basolateral
Apical
Mock
+ SARS-CoV-2
Mock
+ SARS-CoV-2
Mock
+ SARS-CoV-2
110kDa
50kDa
37kDa
ICAM-1
NP
GAPDH
E
ICAM-1 expression
mock
+SARS-CoV-2
Intensity corrected for GAPDH (a.u.)
*
Apical
Basolateral
Apical
HMVEC-L
Calu-3
F
CXCL10 secretion
mock
+SARS-CoV-2
CXCL10 (ng/mL)
Apical
Basolateral
Site of infection
G
IL6 secretion
mock
+SARS-CoV-2
IL6 (ng/mL)
*
*
Apical
Basolateral
Site of infection

Figure 6

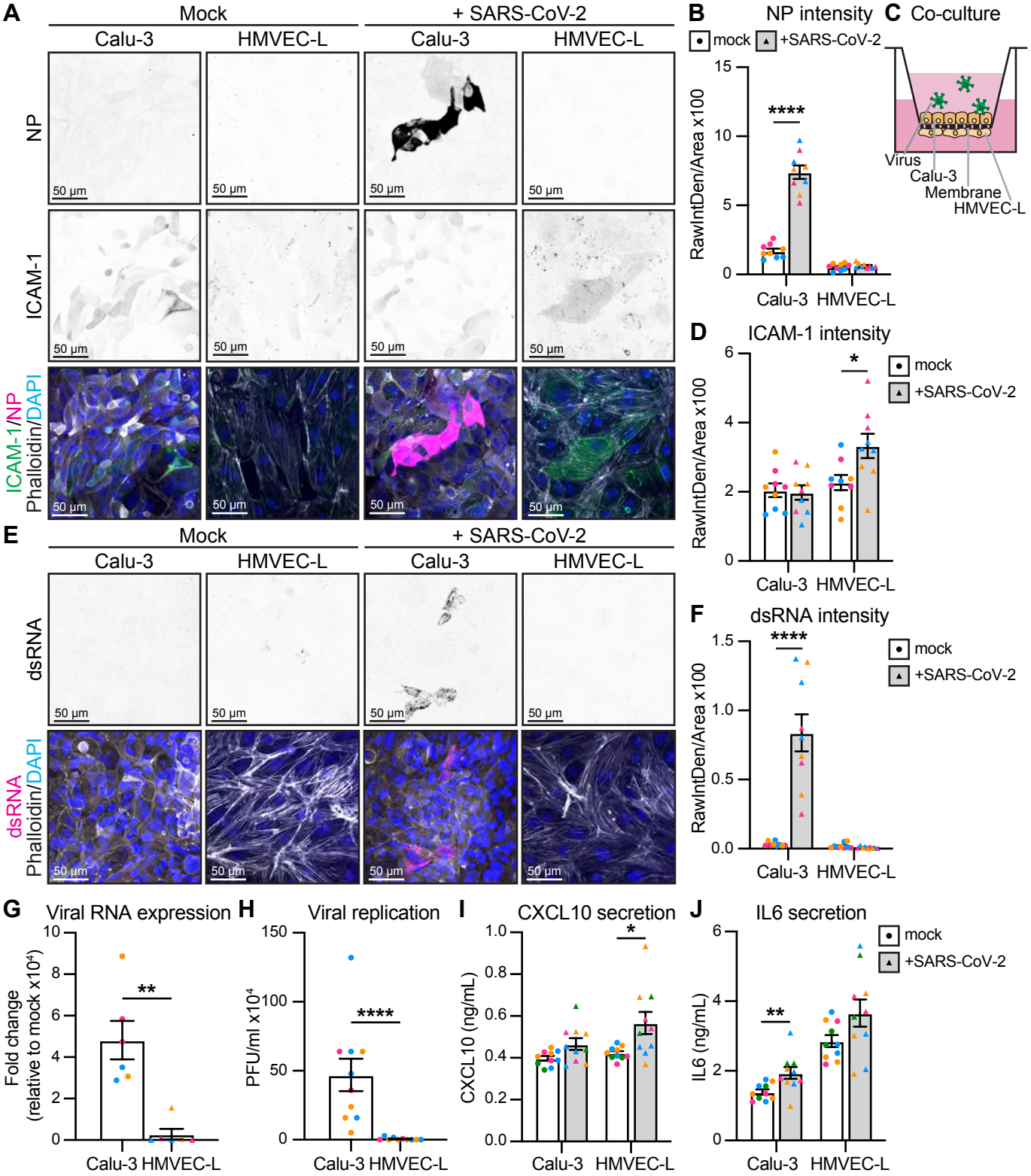
A
Mock
+ SARS-CoV-2
Calu-3
HMVEC-L
NP
ICAM-1
ICAM-1/NP
Phalloidin/DAPI
50 µm
B
NP intensity
mock
+SARS-CoV-2
RawIntDen/Area x100
****
C
Co-culture
Virus
Calu-3
Membrane
HMVEC-L
D
ICAM-1 intensity
*
E
dsRNA
dsRNA
Phalloidin/DAPI
F
dsRNA intensity
G
Viral RNA expression
Fold change
(relative to mock x10⁴)
**
H
Viral replication
PFU/ml x10⁴
I
CXCL10 secretion
CXCL10 (ng/mL)
J
IL6 secretion
IL6 (ng/mL)
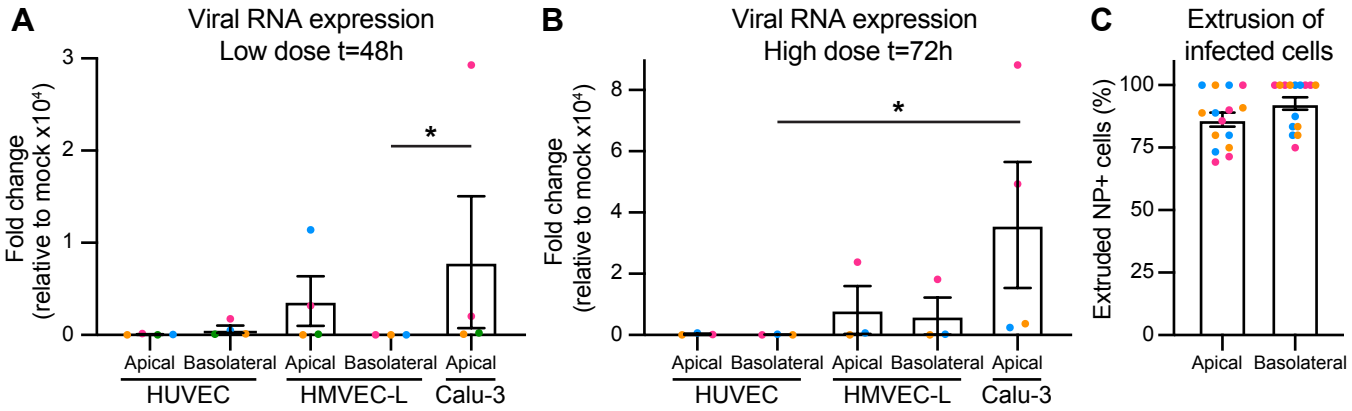
Supplemental Figure 1